Supporting Information

On the understanding of the optoelectronic properties of S-doped MoO_3 and O-doped MoS_2 bulk systems: A DFT Perspective

Masoud Shahrokhi [1], Pascal Raybaud [1,2] and Tangui Le Bahers [1]

[1]*Univ Lyon, ENS de Lyon, CNRS, Université Claude Bernard Lyon 1, Laboratoire de Chimie UMR 5182, F-69342 Lyon, France*

[2]*IFP Energies nouvelles, Rond-point de l'échangeur de Solaize, BP 3, 69360 Solaize, France*

1. Optimizing the Grimme D3 scaling factor

In the D3 correction method of Grimme et al. [1], the following vdW-energy expression is used:

$$E_{disp} = -\frac{1}{2}\sum_{i=1}^{N_{at}}\sum_{j=1}^{N_{at}}\sum_{L}{}'\left(f_{d,6}(r_{ij,L})\frac{C_{6ij}}{r_{ij,L}^{6}} + f_{d,8}(r_{ij,L})\frac{C_{8ij}}{r_{ij,L}^{8}}\right) \quad (1)$$

In the zero damping D3 method for short ranges, damping of the following form is used:

$$f_{d,n}(r_{ij}) = \frac{S_n}{1+6(r_{ij}/(s_{R,n}R_{0ij}))^{-\alpha_n}} \quad (2)$$

where $R_{0ij} = \sqrt{\frac{C_{8ij}}{C_{6ij}}}$. In CRYSTAL S_6 and S_8 parameters with default values of 1.00 and 1.2177, respectively, are adjustable parameters. First, we reduce both S_6 and S_8 parameters by 10% and we continue this trend down to 100%. For each S_6 and S_8 parameters we optimized the structures of pristine α-MoO_3 and 2H-MoS_2 and obtained lattice parameters. For 2H-MoS_2 system our results confirmed that in different S_6 and S_8 parameters, the in-plane lattice parameter (*a*) difference is small (from 3.13 Å for 0.00% reduction to 3.16 Å for 100% reduction) while the out-of-plane lattice parameter is changed dramatically (from 11.80 Å for 0.00% and 12.70 Å for 100%).

The closest out-of-plane lattice parameter for MoS_2 to the experimental results (12.29 Å [2]) obtained for 70% reduction of S_6 and S_8 parameters which is 12.28 Å. We also performed the same calculations for similar layered structures such as hexagonal BN with P63/mmc space group (#194), gt-C_3N_4 with $P6_3/m$ space group (#176) and gh-C_3N_4 with Fd_3m space group (#227). For all aforementioned systems reduction of S_6 and S_8 parameters in the range of 60%-80% leads to the best out-of-plane lattice parameter in comparison with experiment (Figure S1).

The same calculations for α-MoO_3 showed that the default values of S_6 and S_8 parameters lead to the closest out-of-plane lattice parameter to the experiment. Hence, for 2H-MoS_2 structures the Grimme D3 approach was used with 70% reduction of S_6 and S_8 parameters (S_6=0.30 and S_8=0.37) while for α-MoO_3 we used the default values (S_6=1.00 and S_8=1.2177).

For doped materials, the S_6 and S_8 parameters optimized for the pristine structures were used. Another strategy would be to use a dispersion correction self-consistently adapted to the material, such as the dDsC approach [3,4]. But for this investigation, only the tuned D3 correction was considered.

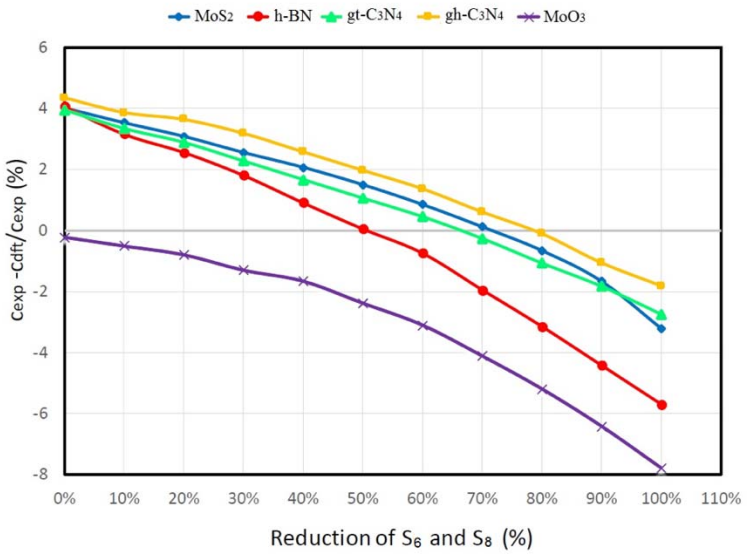

Figure S1. Optimized out-of-plane lattice parameter of 2H-MoS_2, h-BN, gt-C_3N_4, gh-C_3N_4 and α-MoO_3 structures for different S_6 and S_8 parameters of Grimme D3 approach.

2. Geometry of α-MoO_3 and 2H-MoS_2 bulk systems

The calculated lattice parameters for the primitive orthorhombic bulk unit-cell of α-MoO_3, optimized using PBE and DFT-D3 (a_{calc} = 13.90, b_{calc} = 3.72, and c_{calc} = 3.94 Å), agree well with the experimental data (a_{exp} = 13.87, b_{exp} = 3.70, and c_{exp} = 3.96 Å) [5].

Each layer of α-MoO_3 bulk consists of two sublayers including three distinct types of oxygen atoms: terminal (singly coordinated, O_t), asymmetrical (doubly coordinated, O_a), and symmetrical (triply coordinated, O_s) oxygen atoms while all S atoms in 2H-MoS_2 structure are equivalent (Fig. 1 (a)) [6, 7]. The O_t links to a single Mo atom which is the shortest bond length (1.69 Å) in the α-MoO_3 bulk. The O_a atom is 2-fold as it links to two Mo atoms in the same sublayer with one long (2.20 Å) and one short (1.77 Å) bonds. The O_s is 3-fold by forming two equal Mo-O bonds (1.96 Å) in the same sublayer and one longer Mo-O bond (2.47 Å) which connects two sublayers. The simulated lattice parameters for the primitive bulk cell of 2H-MoS_2 using PBE and DFT-D3 dispersion correction with

optimized D3 scaling factors are a_{calc} = 3.16, and c_{calc} = 12.28 Å, in an excellent agreement with the experimental values (a_{exp} = 3.16, and c_{exp} = 12.29 Å [2]). The Mo-S bond length in this system is 2.41 Å. Fig. 1 (a) and (b) illustrates the unit-cell structure of α-MoO_3 and 2H-MoS_2, respectively.

2.1. Sulfur-doped α-MoO_3 with different concentrations

To study the effects of sulfur doped α-MoO_3 and oxygen doped 2H-MoS_2 structures, different dopant concentrations were considered for both systems. To this aim, a host unit-cell structure of aforementioned systems was adopted for high dopant concentration levels while different size supercells were used for low concentration levels. At the first step, for the lowest S concentration, a 2 × 2 × 2 α-MoO_3 host supercell that consists of 32 Mo atoms and 96 O atoms was used to simulate the anionic doped $MoO_{3-x}S_x$ (Fig. S2). Each layer of α-MoO_3 bulk system consists of two sublayers and there are three distinct types of oxygen atoms in each sublayer: terminal (O_t), asymmetrical (O_a), and symmetrical (O_s) oxygen atoms (Fig. 1). Substituting one sulfur atom into the three oxygen site variants (O_t, O_a and O_s) of 2 × 2 × 2 MoO_3 supercell leads to three *mono*-atomic S-doped structures with the concentration of 1.04% and $MoO_{2.97}(S_t)_{0.03}$, $MoO_{2.97}(S_a)_{0.03}$ and $MoO_{2.97}(S_s)_{0.03}$ chemical formula. In all oxygen sites, the bond length of Mo-S is greater than Mo-O because S has a larger ionic radius.

To evaluate the stability of these structures, the formation energies per MoO_3 of S-doped α-MoO_3 supercell were computed as

$$E_f = \left(\frac{E_{tot} - (n_{Mo}E_{Mo} + (\frac{1}{2})n_O E_{O_2} + n_S E_{S_\alpha})}{N} \right) \times 4 \quad (3)$$

where E_{tot} is the total energy per cell, E_i is the energy of the *i*-th individual elements in their respective ground states, n_i is the number of species i in the structure and N is the total number of atoms per cell. The calculated formation energy for α-MoO_3 is -8.20 eV (without ZPE and thermal corrections) which is comparable to the experimental formation enthalpies -7.72 eV per MoO_3 (according to the PBE-D3 functional used). The formation energy of these materials increases of the sulfur-doped MoO_3 materials by using the conventional reference states, solid sulfur (α-sulfur) and isolated O_2.

At this lowest S-concentration, the calculated formation energies show that the three *mono*-S substituted structures, $MoO_{2.97}(S_t)_{0.03}$, $MoO_{2.97}(S_a)_{0.03}$, and $MoO_{2.97}(S_s)_{0.03}$ are equivalent: E_f = -8.00 eV, -7.96 and -7.96 respectively.

To probe the relative stability of α-MoO_3 structure which O atoms in a sublayer are fully-substituted by S-atoms versus the partially-substituted, an 8 × 1 × 1 supercell with 32 Mo atoms and 96 O atoms ($MoO_{2.97}(S_t)_{0.03}$ with the same S concentration of 1.04%) have been also considered (Fig. S2 (d)). The comparison of the formation energies for 8 × 1 × 1 supercell and the previous 2 × 2 × 2 supercell with one S_t-doped confirms that system with fully S-doped in one sublayer is more stable than the partially S-doped one by about -0.12 eV for E_f.

In addition, to examine how the S-doping atoms localization (S_t, S_a, S_s) is affected by the concentration, we also considered the higher concentration of 8.33% for $MoO_{2.75}(S_t)_{0.25}$, $MoO_{2.75}(S_a)_{0.25}$, and $MoO_{2.75}(S_s)_{0.25}$ chemical formula (Fig. S3). It is unveiled that again the formation energies are rather close: $MoO_{2.75}(S_t)_{0.25}$ with E_f = -7.48 eV is slightly more stable than $MoO_{2.75}(S_a)_{0.25}$, and $MoO_{2.75}(S_s)_{0.25}$ structures with E_f = -7.28 and -7.32 eV. These results indicate that the S_t site may be the most favorite site for low and high concentrations. Because substitution along the direction including vdW gap exhibits the largest lattice constant and can, therefore, accommodate the S impurity with less strain. The Mo-S_t bond length in S-doped MoO_3 systems is ~ 2.13 Å which is 0.44 Å greater than the Mo-O_t bond length.

We also consider S-doped structures for intermediate concentrations of 2.08% and 4.16%. For x_s = 2.08% (with $MoO_{2.94}(S_t)_{0.06}$ chemical formula) two supercell structures of 1 × 2 × 2 and 4 × 1 × 1 MoO_3 which consist of 16 Mo atoms and 48 O atoms were chosen. For x_s = 4.16% (with $MoO_{2.87}(S_t)_{0.13}$ chemical formula) we used 1 × 2 × 1 and 2 × 1 × 1 supercell structures with 8 Mo atoms and 24 O atoms. Since the S_t site is the most favorite site for S-substituted α-MoO_3, only this position of dopant atoms was studied for these supercell structures. In both 1 × 2 × 2 and 1 × 2 × 1 supercells, sulfur doping leads to one sublayer of MoO_3 structure partially substituted by S_t atoms while in 4 × 1 × 1 and 2 × 1 × 1 supercells one sublayer of MoO_3 structure is fully substituted by S_t atoms (Fig. S4 (a-d)). Our results also confirm that the structures in which a sublayer is fully substituted by S atoms are slightly more stable than partially S-substituted ones (Table S1).

For higher concentration levels, x_s = 16.66% (with $MoO_{2,50}(S)_{0,50}$ chemical formula), the uniform (two similar O sites were replaced by S atoms) and non-uniform (two different O sites were replaced by S atoms) doping configurations were considered. It is found that the structures with uniform doping which both S atoms substituting for the two O_t sites are more stable than those structures (Fig. S5). Moreover, among all uniform S doping configurations, the structure with two S_t in consecutive layers, which are at the nearest distance one from each other, is the most stable one (Fig. S5 (c)).

A MoO_3 unit-cell structure was used to study S-doped structures for even higher concentration of 25.00% (with $MoO_{2.75}(S_t)_{0.25}$ chemical formula) and 33.00%. (with $MoO_2(S_t)$ chemical formula) (Fig. S6). The E_f value for x_s = 25.00% is -6.44 eV while it is -5.80 eV for x_s = 33.00%.

From Table S1 it is obvious that by increasing sulfur concentration the lattice parameters along directions including vdW gap (*a*) is increased while the in-plane lattice parameters (*b* and *c*) remain almost unchanged. It can also be seen that by increasing the S concentration level, the formation energy of these materials increases which leads to their stability reduction.

S concentration (%)	System	corresponding cell	corresponding figure	*k-point mesh*	*a* (Å)	*b* (Å)	*c* (Å)	E_f (eV)	ΔE_f (eV)	E_g *(eV)*
0.0	MoO_3	unitcell	Fig. 1 (a)	8×12×12	13.90	3.72	3.94	-8.20	0.00	2.96
1.04	$MoO_{2.97}(S_t)_{0.03}$	(2 × 2 × 2)	Fig. S2 (a)	4×6×6	14.16	3.71	3.94	-8.00	0.12	2.12
	$MoO_{2.97}(S_a)_{0.03}$	(2 × 2 × 2)	Fig. S2 (b)	4×6×6	13.89	3.71	3.98	-7.96	0.16	1.71
	$MoO_{2.97}(S_s)_{0.03}$	(2 × 2 × 2)	Fig. S2 (c)	4×6×6	14.02	3.72	3.94	-7.96	0.16	1.53
	$MoO_{2.97}(S_t)_{0.03}$	(8 × 1 × 1)	Fig. S2 (d)	1×12×12	14.12	3.71	3.78	-8.12	0.00	1.62
2.08	$MoO_{2.94}(S_t)_{0.06}$	(4 × 1 × 1)	Fig. S4 (a)	2×12×12	14.45	3.70	3.79	-8.00	0.00	1.62
	$MoO_{2.94}(S_t)_{0.06}$	(1 × 2 × 2)	Fig. S4 (b)	8×6×6	14.39	3.71	3.94	-7.88	0.12	2.14
4.16	$MoO_{2.87}(S_t)_{0.13}$	(2 × 1× 1)	Fig. S4 (c)	4×12×12	14.57	3.72	3.92	-7.80	0.00	1.61
	$MoO_{2.87}(S_t)_{0.13}$	(1× 2× 1)	Fig. S4 (d)	8×6×12	14.78	3.71	3.94	-7.76	0.04	1.93
8.33	$MoO_{2.75}(S_t)_{0.25}$	unit-cell	Fig. S3 (a)	8×12×12	15.22	3.72	3.93	-7.48	0.00	1.69
	$MoO_{2.75}(S_a)_{0.25}$	unit-cell	Fig. S3 (b)	8×12×12	15.28	3.76	3.90	-7.28	0.20	1.70
	$MoO_{2.75}(S_s)_{0.25}$	unit-cell	Fig. S3 (c)	8×12×12	15.34	3.70	3.96	-7.32	0.16	1.92
16.66	$MoO_{2.50}(S_t)_{0.50}$	unit-cell	Fig. S5 (a)	8×12×12	16.53	3.72	3.92	-6.68	0.32	1.43
	$MoO_{2.50}(S_t)_{0.50}$	unit-cell	Fig. S5 (b)	8×12×12	16.55	3.72	3.92	-6.96	0.04	1.86
	$MoO_{2.50}(S_t)_{0.50}$	unit-cell	Fig. S5 (c)	8×12×12	15.92	3.72	3.94	-7.00	0.00	1.87
25.00	$MoO_{2.25}(S_t)_{0.75}$	unit-cell	Fig. S6 (a)	8×12×12	17.32	3.72	3.93	-6.44	0.00	1.63
33.00	MoO_2S	unit-cell	Fig. S6 (b)	8×12×12	17.87	3.72	3.94	-5.80	0.00	1.80

Table S1. Different models, corresponding figures, *k*-point mesh, calculated optimized lattice parameters, formation energy (E_f) per MoO_3 and the difference in formation energy between each structure and the most stable one (ΔE_f) and the electronic band gap (E_g) for the S-substituted MoO_3 bulk for different concentrations.

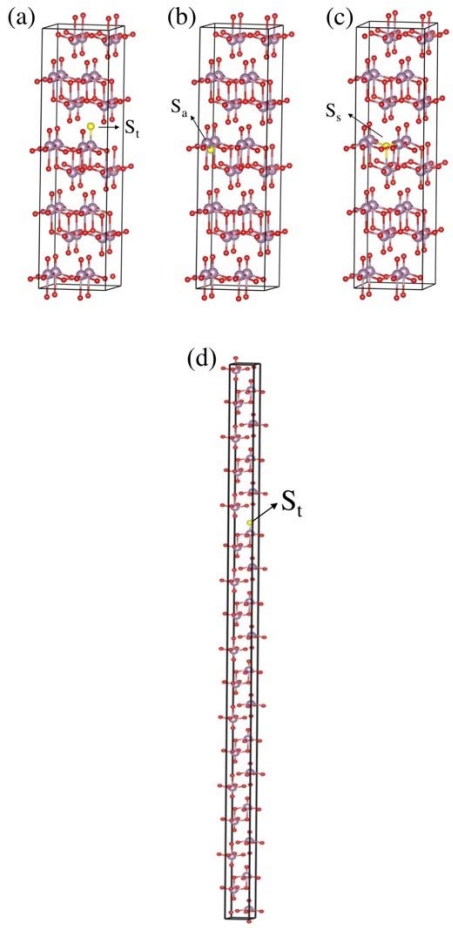

Figure S2. Optimized structures of (2 × 2 × 2) and (8 × 1 × 1) supercells for the bulk α-MoO_3 which one O site (O_t, O_a or O_s) was replaced by S atom (x_s = 1.04%) with $MoO_{2.97}(S)_{0.03}$ chemical formula. The purple, red and yellow balls in the geometrical models represent the Mo, O and S atoms, respectively.

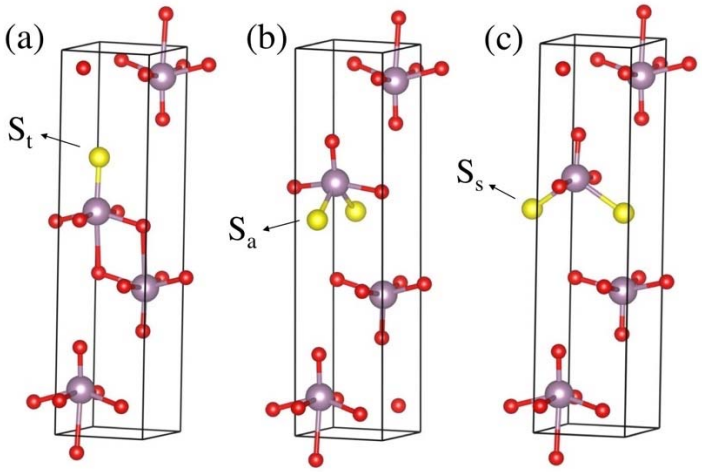

Figure S3. Optimized structures of S-doped α-MoO_3 unit-cell (x_s = 8.33%) for different configurations: $MoO_{2.75}(S_t)_{0.25}$ (a), $MoO_{2.75}(S_a)_{0.25}$ (b), and $MoO_{2.75}(S_s)_{0.25}$ (c). Color code as in Figure S2.

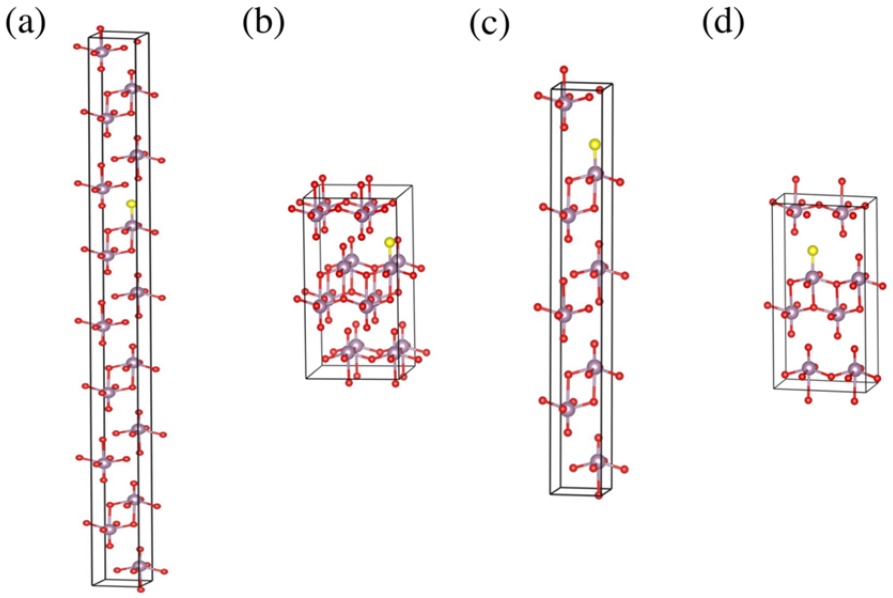

Figure S4. Optimized structures of S-substituted (a) (4 × 1× 1) and (b) (1 × 2 × 2) supercells of α-MoO_3 with the S doped for x_s = 2.08% (with $MoO_{2.94}(S_t)_{0.06}$ chemical formula). (c) (2 × 1 × 1) and (d) (1 × 2 × 1) supercells of α-MoO_3 with S doped for x_s = 4.16% (with $MoO_{2.87}$ $(S_t)_{0.13}$ chemical formula). Color code as in Figure S2.

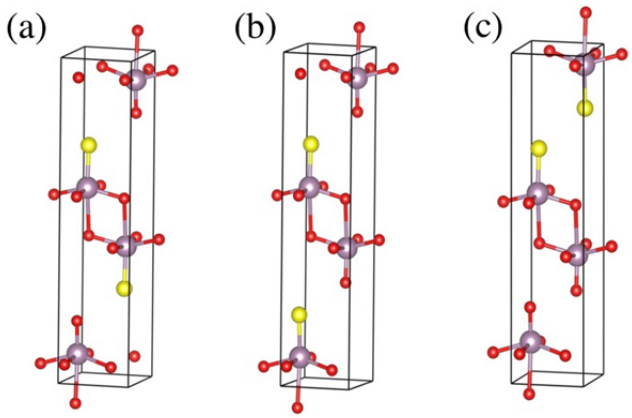

Figure S5. Optimized structures of S-doped α-MoO_3 unit-cell for x_s = 16.66% ($MoO_{2.50}(S_t)_{0.50}$) with uniform doping which both S atoms substituting for the two different O_t sites. Color code as in Figure S2.

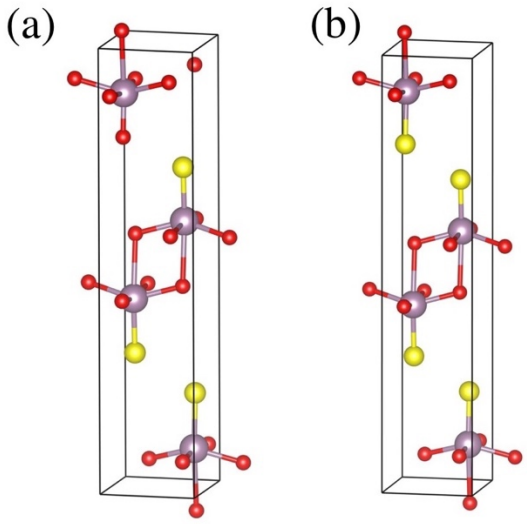

Figure S6. Optimized structures of S-doped α-MoO_3 unit-cell for (a) x_s = 25.00% ($MoO_{2.25}(S_t)_{0.75}$) and (b) x_s = 33.00% ($MoO_2(S_t)$) with uniform doping which all S atoms substituting for the O_t sites. Color code as in Figure S2.

2.2. Oxygen-doped 2H-MoS_2 with different concentrations

The O-doping in 2H-MoS_2 bulk was simulated by substituting S atoms with equal number of O atoms in different concentrations. For low concentrations O-doped 2H-MoS_2 bulk system two different supercells were studied: (2 × 2 × 2) supercell that consists of 16 Mo atoms and 32 S atoms for x_O = 3.13 and 6.25% and (2 × 2 × 1) supercell that consists of 8 Mo atoms and 16 S atoms for x_O = 6.25%, x_O = 12.50%, x_O = 25.00%, x_O = 33.50%, x_O = 50.00%, x_O = 62.50% and x_O = 75.00%. We also use

the unit-cell of MoS_2 system for x_O = 25.00%, 50.00% and 75.00% (which a layer of MoS_2 is fully substituted by O atoms).

The formation energies per MoS_2 of O-doped 2H-MoS_2 supercell were computed as

$$E_f = \left(\frac{E_{tot} - (n_{Mo}E_{Mo} + n_S E_{S\alpha} + (\frac{1}{2})n_O E_{O2})}{N} \right) \times 3 \quad (4)$$

For pristine MoS_2, the formation energy is -2.28 eV per MoS_2 in reasonable agreement with the experimental formation enthalpy (-2.96 eV) and the formation energy of O-doped MoS_2 systems decreases as a function of O content.

For the lowest concentration, x_O = 3.13% one S atom in the (2 × 2 × 2) supercell is substituted by O atoms lead to $MoS_{1.94}O_{0.06}$ systems (Fig. S7 (a)). For x_O = 6.25%, two different systems were tested: in the (2 × 2 × 2) supercell two S atoms are substituted by two O atoms and in the (2 × 2 × 1) supercell one S atom is substituted by O atom lead to $MoS_{1.87}O_{0.13}$ (Fig. S7 (b) and (c)). Our results show that the (2 × 2 × 2) supercell structure with two substituted O which the second O atom is located below the first substituted oxygen is energetically more favorable.

For x_O = 12.50% six different configurations were considered which two sulfur sites of (2 × 2 × 1) supercell replaced by O atoms: two O atoms were substituted in the same layer (Fig. S7 (d-f)) and two O atoms were substituted in different layers (Fig. S7 (g-i)). We found that configuration (f) from Fig. S7 is the most stable structure for x_O = 12.50% which the second O atom tended to substitute the S atom located below the first substituent O atom. However, the corresponding relative energies for all configurations listed in Table S2 reveal that they are all very close in energy.

To study x_O = 25.00%, we used two different size structures: a (2 × 2 × 1) supercell with four O-substituted in different layers that each O located below its counterpart atom in the same layer (Fig. S7 (j)) and a unit-cell with one O atom substituting for one S site (Fig. S8 (a)). The formation energies indicate that for dopant concentration of 25.00% a (2 × 2 × 1) supercell of MoS_2 with four O-substituted is more stable than a unit-cell with one O atom substituting for one S site. These results

confirm that the MoS_2 structures in which one single layer is fully substituted by oxygen atoms are slightly less stable than partially O-substituted ones which is in contrast with what was observed for S-doped MoO_3 systems.

Substituting six and ten oxygen atoms of the (2 × 2 × 1) supercell yields x_O = 37.50% and x_O = 62.50%, respectively (Fig. S7 (k) and Fig. S7 (m)).

For x_O = 50.00% we also used two different size structures: a (2 × 2 × 1) supercell with eight O-substituted that each O located below its counterpart atom in the same layer (Fig. S7 (l)) and a unit-cell of MoS_2 with three different dopant configurations that two O atoms substituting for two sulfur sites (Fig. S8 (b-d)). It is found that among all O-substituted MoS_2 unit-cell configurations, the structure with two O in different layers, which are at the farthest distance from each other, is stable than other configurations (Fig. S8 (b)). Nevertheless, for dopant concentration of 50.00% a (2 × 2 × 1) supercell of MoS_2 with eight O-substituted is more stable than all unit-cell configurations substituted with two O atoms.

Two different size cells were designed to study the greatest concentration of doping effect (x_O = 75.00%): a (2 × 2 × 1) supercell substituted with twelve O atoms (Fig. S7 (n)) and a unit-cell of MoS_2 substituted with three O atoms (Fig. S8 (e)). Our results show that a (2 × 2 × 1) supercell of MoS_2 with twelve O-substituted is more stable than the unit-cell configurations substituted with three O atoms.

It can be concluded that both in-plane and out-of-plane lattice parameters of MoS_2 are reduced by increasing oxygen concentration level. The Mo-O bond length in all substituted systems is ~ 2.08 Å and smaller than Mo-S bond length. Our results confirm that fully substituting S atoms with O atoms in a layer of MoS_2 system is less stable than partially O-substituted ones. It is also revealed that by increasing the O concentration, the formation energy of these materials decreases leading to the stability enhancement for O-doped MoS_2 systems.

O concentration (%)	System	corresponding cell	figure	*k-point mesh*	*a* (Å)	*c* (Å)	E_f (eV)	ΔE_f (eV)	E_g *(eV)*
0.0	MoS_2	unit-cell	Fig. 1 (b)	12×12×8	3.16	12.28	-2.28	0.00	1.56
3.13	$MoS_{1.94}O_{0.06}$	(2 × 2 × 2)	Fig. S7 (a)	6×6×4	3.14	12.28	-2.34	0.00	1.50
6.25	$MoS_{1.87}O_{0.13}$	(2 × 2 × 2)	Fig. S7 (b)	6×6×4	3.13	12.27	-2.43	0.00	1.54
		(2 × 2 × 1)	Fig. S7 (c)	6×6×8	3.13	12.31	-2.40	0.03	1.53
12.50	$MoS_{1.75}O_{0.25}$	(2 × 2 × 1)	Fig. S7 (d)	6×6×8	3.11	12.28	-2.46	0.12	1.44
			Fig. S7 (e)		3.10	12.36	-2.52	0.06	1.42
			Fig. S7 (f)		3.11	12.28	-2.58	0.00	1.38
			Fig. S7 (g)		3.11	12.33	-2.55	0.03	1.53
			Fig. S7 (h)		3.11	12.36	-2.55	0.03	1.54
			Fig. S7 (i)		3.11	12.33	-2.55	0.03	1.57
25.00	$MoS_{1.50}O_{0.50}$	(2 × 2 × 1)	Fig. S7 (j)	6×6×8	3.07	12.25	-2.94	0.00	1.57
		unit-cell	Fig. S8 (a)	12×12×8	3.07	11.78	-2.82	0.12	1.03
37.50	$MoS_{1.25}O_{0.75}$	(2 × 2 × 1)	Fig. S7 (k)	6×6×8	3.02	12.16	-3.30	0.00	1.38
50.00	MoSO	(2 × 2 × 1)	Fig. S7 (l)	6×6×8	2.98	12.20	-3.69	0.00	1.71
		unit-cell	Fig. S8 (b)	12×12×8	2.98	11.15	-3.54	0.15	1.55
		unit-cell	Fig. S8 (c)	12×12×8	2.97	11.39	-3.42	0.27	0.05
		unit-cell	Fig. S8 (d)	12×12×8	2.98	11.11	-3.51	0.18	1.41
62.50	$MoS_{0.75}O_{1.25}$	(2 × 2 × 1)	Fig. S7 (m)	6×6×8	2.95	11.44	-4.08	0.00	1.12
75.00	$MoS_{0.50}O_{1.50}$	(2 × 2 × 1)	Fig. S7 (n)	6×6×8	2.90	11.34	-4.50	0.00	1.57
		unit-cell	Fig. S8 (e)	12×12×8	2.90	10.66	-4.32	0.18	0.37

Table S2. Different models, corresponding figures, *k*-point mesh, calculated optimized lattice parameters, formation energy (E_f) per MoS_2, the difference in formation energy between each structure and the most stable one (ΔE_f) and the electronic band gap (E_g) for the O-substituted MoS_2 bulk for different concentrations.

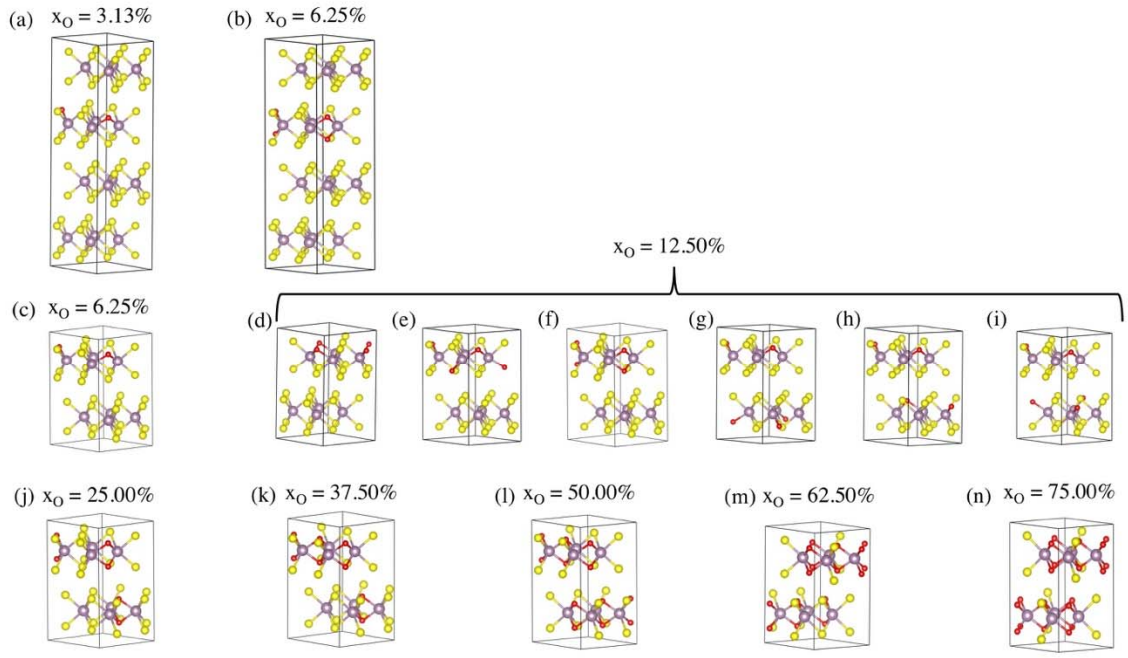

Figure S7. Optimized structures of O-doped 2H-MoS_2 bulk: (a) (2 × 2 × 2) supercell of bulk MoS_2 with x_O = 3.13% ($MoS_{1.94}O_{0.06}$), (b) (2 × 2 × 2) supercell of bulk MoS_2 with x_O = 6.25% ($MoS_{1.87}O_{0.13}$), (c) (2 × 2 × 1) supercell of bulk MoS_2 with x_O = 6.25% ($MoS_{1.87}O_{0.13}$), (d-i) (2 × 2 × 1) supercell of bulk MoS_2 with x_O = 12.50% ($MoS_{1.75}O_{0.25}$), (j) (2 × 2 × 1) supercell of bulk MoS_2 with x_O = 25.00% ($MoS_{1.50}O_{0.50}$), (k) (2 × 2 × 1) supercell of bulk MoS_2 with x_O = 37.50% ($MoS_{1.25}O_{0.75}$), (l) (2 × 2 × 1) supercell of bulk MoS_2 with x_O = 50.00% (MoSO), (m) (2 × 2 × 1) supercell of bulk MoS_2 with x_O = 62.50% ($MoS_{0.75}O_{1.25}$) and (n) (2 × 2 × 1) supercell of bulk MoS_2 with x_O = 75.00% ($MoS_{0.50}O_{1.50}$). Color code as in Figure S2.

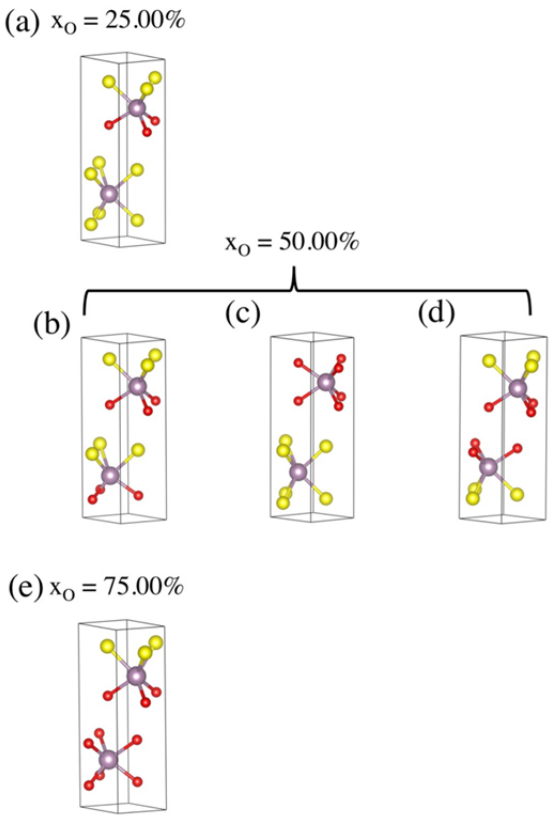

Figure S8. Optimized structures of (a) MoS_2 unit-cell with x_O = 25.00% ($MoS_{1.50}O_{0.50}$), (b, c and d) MoS_2 unit-cell with x_O = 50.00% (MoSO) and (e) MoS_2 unit-cell with x_O = 75.00% ($MoS_{0.50}O_{1.50}$). Color code as in Figure S2.

2.3. Thermodynamic analysis

Fig. S9 illustrates the calculated reaction energies corresponding to chemical equations 1 and 2 of the main text, for the most stable S-substituted α-MoO_3 and O-substituted 2H-MoS_2 bulk structures for different concentrations. In this figure, ΔE is the difference of 0K formation energy of the S-substituted α-MoO_3 and O-substituted 2H-MoS_2 systems with respect to DFT formation energies of H_2S and H_2O as reactants/products:

$$\Delta E = E_f(MoO_{3-x}S_x) - E_f(MoO_3) + xE_f(H_2O) - xE_f(H_2S) \quad (5)$$

ΔG is the difference of formation energy of the S-substituted α-MoO_3 and O-substituted 2H-MoS_2 systems with respect to experimental free energies (enthalpy and entropy) of H_2S and H_2O given by NIST thermodynamic database:

$$\Delta G = E_f(MoO_{3-x}S_x) - E_f(MoO_3) + xG_f(H_2O) - xG_f(H_2S) \quad (6)$$

We notice that the impact of entropic effects stabilizes slightly the oxidation process of MoS_2 and destabilizes the sulfidation of MoO_3. However, it does not change the main trend for the temperature of 298 K. The reaction energies for the oxidation of MoS_2 are continuously increasing as a function of x, while the sulfidation energies of MoO_3 are fluctuating between 0 and 0.2 eV. This reveals that the sulfidation process of MoO_3 is thermodynamically more favorable than the oxidation one MoS_2 when we consider H_2S/H_2O as reactants or products.

The full MoO_3/MoS_2 inter-conversion can be written as follows:

$MoO_3 + 2H_2S + H_2 = MoS_2 + 3H_2O$ (7)

Investigating the effect of H_2 is beyond the scope of the present work and we assume here that the controlled conditions of synthesis or reactions will not allow to minimize the H_2 pressure in order to avoid the full transformation. Nevertheless, the calculated reaction energy for (7) is -1.25 eV which indicates that the process is thermodynamic favored. However, the reverse reaction (full oxidation of MoS_2 in MoO_3) is thermodynamically limited. This is coherent with the partial sulfidation or oxidation reaction energies reported in Figure S9. In the present work, we consider that the conditions could be found to avoid the transformation of MoO_3 into MoS_2 only if no hydrogen is added in the reaction medium.

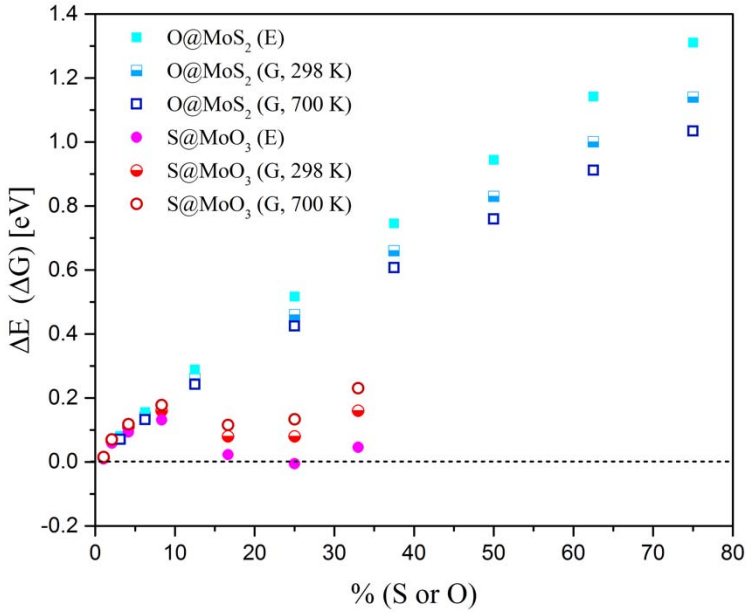

Figure S9. The calculated reaction energy according to equations (5) and (6) for the most stable S-substituted α-MoO_3 and O-substituted 2H-MoS_2 bulk structures for different concentrations.

As an alternative pathway for the oxidation of MoS_2, we can use O_2/SO_2:

$MoS_2 + 3/2xO_2 = MoS_{(2-x)}O_x + xSO_2$ (7)

Neglecting the entropic changes for the solid phases, the Grand potential can be approximated as follows:

$$\Omega_{MoS_{2-x}O_x} = E_f(MoS_{2-x}O_x) - E_f(MoS_2) + xG^0_{f,T_0}(SO_2) - 3/2xG^0_{f,T_0}(O_2) - xRT_0\ln\left[\frac{p(O_2)^{3/2}}{p(SO_2){p_0}^{1/2}}\right]$$

(8)

We can easily show that the new thermodynamic diagram is transformed according to Figure S10 which reveals that the chemical potential of O_2 required for oxidizing MoS_2 is very low in comparison to H_2O. Note also that the full conversion of MoS_2 into MoO_3 is strongly exothermic process, which makes more difficult the control of the partial sulfidation state under O_2/SO_2 environment than under H_2O/H_2S.

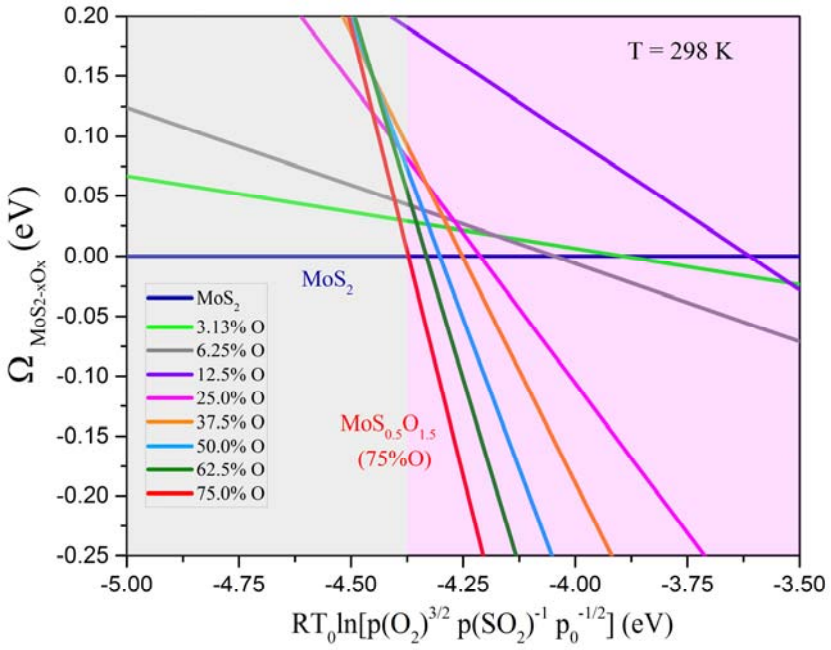

Figure S10. Thermodynamic phase stability of the O-substituted 2H-MoS_2 bulk structures for different O-concentrations with respect to pristine structure considering O_2 and SO_2.

2.4. Analysis of the bonding character

In order to analyze the bonding character between Mo and S (O) atoms, the q_e (total charge) per atom transfer from Mo to S (O) have been calculated by the Bader charge analysis [8]. It is revealed that in pristine MoO_3 crystal, each O_t gains 0.6 electrons from Mo atom while the corresponding value for O_S and O_a is 0.94 and 0.79 electrons, resulting in a net gain of 2.40 electrons on O atoms due to the stoichiometry of the crystal. By substituting one S for O_t atom in the $MoO_{2.75}(S_t)_{0.25}$ crystal, the net charge transferred from Mo to oxygens and sulfur atoms is 2.05 electrons which the number of electrons transferred between from Mo to S is ~0.25 electrons. It is also found that an average electron transfer of 1.0 from each Mo to its nearest S neighbors in pristine MoS_2 bulk, resulting in a net gain of 0.5 electrons on S due to the stoichiometry of the crystal. In $MoS_{1.75}O_{0.25}$ system, the net charge transferred to oxygen atom is 0.89 electrons which is greater than that for sulfur atoms. In both cases, by decreasing the atomic radii of oxygen in comparison with sulfur, and consequently increasing oxygen electronegativity, the covalent character of the bond decrease and a small proportion of ionic

bond appear. To gain a better understanding of the bonding characters, we have calculated the difference in charge density (i.e., the crystal density minus the superposition of isolated atomic densities) of the $MoO_{2.75}(S_t)_{0.25}$ and $MoS_{1.75}O_{0.25}$ crystals as shown in Fig. S11. In both cases, charge transfer is highlighted from Mo atom to S and O atoms. Obviously, electronic charge accumulates mainly between Mo and S atoms which suggests a stronger covalent character of the Mo-S bond. By contrast, a larger electronic charge transfer occurs around O atom with a smaller accumulation between Mo and O which reveals a higher ionic feature of the Mo-O bond in this system.

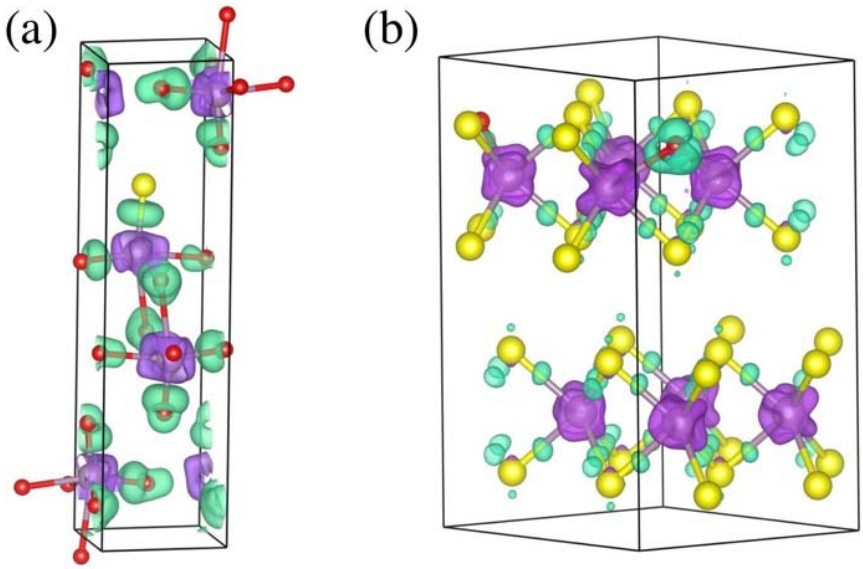

Figure S11. The charge density difference (i.e., the crystal density minus the superposition of isolated atomic densities) in (a) $MoO_{2.75}(S_t)_{0.25}$ and (b) $MoS_{1.75}O_{0.25}$. The green and purple isosurfaces represent the maximum and minimum values at 0.07 and -0.07 a_0^{-3} for $MoO_{2,75}(S_t)_{0,25}$ (0.09 and −0.04 a_0^{-3} for $MoS_{1.75}O_{0.25}$), respectively. Color code as in Figure S2.

3. Electronic properties of Sulfur-doped α-MoO_3 in different concentrations

The valence band maximum (VBM) of the pristine α-MoO_3 occurs at the *T*-point and the conduction band minimum (CBM) is situated at the *Γ*-point, resulting in an indirect band gap. The PDOS in Fig. S12 of α-MoO_3 bulk shows the top of the valence band is dominated by O 2p orbitals, whereas the

bottom of the conduction band is formed from Mo 4d orbitals with weak hybridization of O 2p states resulting in charge-transfer insulator. Moreover, we also find very interesting sites-dependent partial density of states. It can be seen that 2p states of the O_a and O_s oxygens in α-MoO_3 dominate the VBM and the state of CBM is mainly composed of the Mo 4d orbital with very weak hybridization of 2p of O_a atoms. These results indicate that atomic orbitals of in plane oxygens (O_a and O_s) dominated the VBM for α-MoO_3 compound, and CBM state are also mainly contributed by atomic orbital of O_a and Mo atoms.

The band structure of pristine 2H-MoS_2 shows a primary indirect transition where the VBM occurs at the *Γ*-point and the CBM is located along the *Γ*-*K*-direction with a band gap of 1.56 eV (Fig. 3 (b)), corresponding to an overestimation of ~30% compared to the experiment (1.20 and 1.29 eV) [9, 10]. It is worth noting that the experimental value of band gap is optical band gap while the computed one is fundamental electronic band gap (fundamental electronic band gap = optical band gap + exciton binding energy) [11].

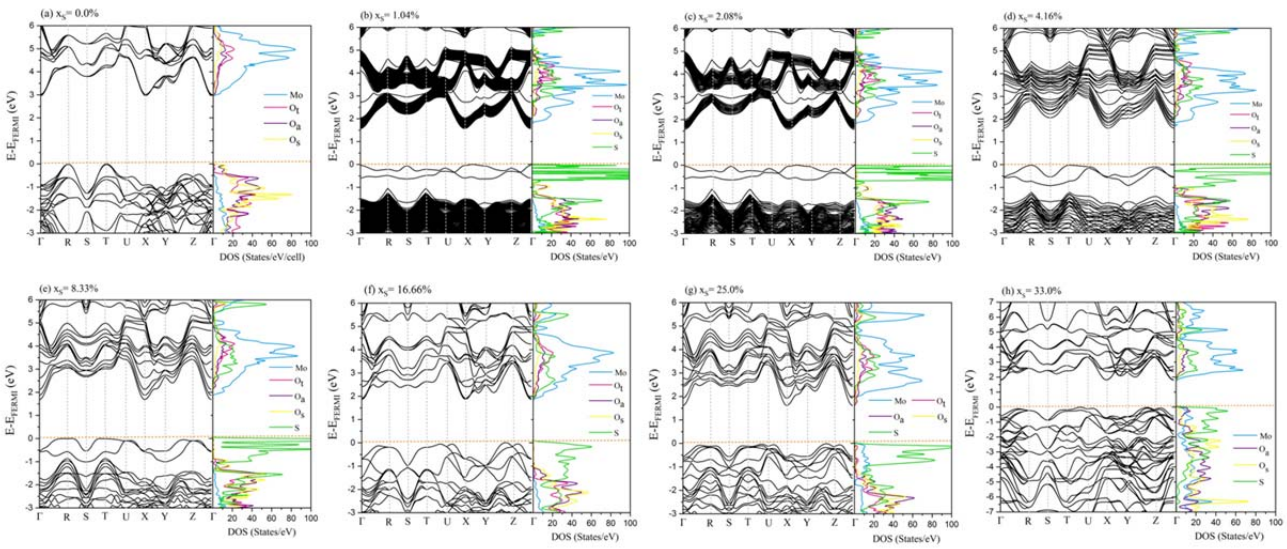

Figure S12. Band structure and PDOS of the most stable S-substituted α-MoO_3 bulk structures for different concentrations calculated using HSE06. The Fermi level is set to zero.

Table S3. DFT calculated band gap energy, effective mass of electron and hole, DOS- averaged effective masses, electron and hole mobility of the most stable S-substituted α-MoO_3 bulk structures for different concentrations.

System	S concentration (%)	E_g (eV)	m_e^{*a} (m_e)	m_h^{*a} (m_e)	$m_{e\ DOS}^{*b}$ (m_e)	$m_{h\ DOS}^{*b}$ (m_e)	μ_e [c] ($cm^2 V^{-1} s^{-1}$)	μ_h [c] ($cm^2 V^{-1} s^{-1}$)
MoO_3	0.0	2.96	0.63	0.40	0.61	1.13	29	16
$MoO_{2.97}S_{0.03}$	1.04	1.62	0.71	0.29	3.78	4.75	5	4
$MoO_{2.94}S_{0.06}$	2.08	1.62	0.70	0.30	2.80	5.60	6	3
$MoO_{2.87}S_{0.13}$	4.16	1.61	0.71	0.23	2.31	1.74	8	10
$MoO_{2.75}S_{0.25}$	8.33	1.69	0.72	0.15	0.95	2.36	19	7
$MoO_{2.50}S_{0.50}$	16.66	1.87	0.66	0.18	0.40	2.55	45	7
$MoO_{2.25}S_{0.75}$	25	1.63	0.71	0.14	1.32	1.86	13	9
MoO_2S	33	1.80	0.68	0.11	0.48	1.77	37	10

[a] Harmonic average of [010], [001] and [011] directions. [b] DOS- averaged effective masses and mobility obtained from the Boltzmann transport theory as implemented in CRYSTAL17 code and calculated at a carrier density of 10^{17} cm^{-3}. [c] The mobility was estimated under the assumption of τ = 10 fs.

The electronic band structures and PDOS for fully and partially S-doped in a sublayer of α-MoO_3 systems have been compared in Fig. S13. It is noteworthy that the partially S-doped in a sublayer of α-MoO_3 bulk leads to larger electronic band gap in comparison with fully S-doped ones.

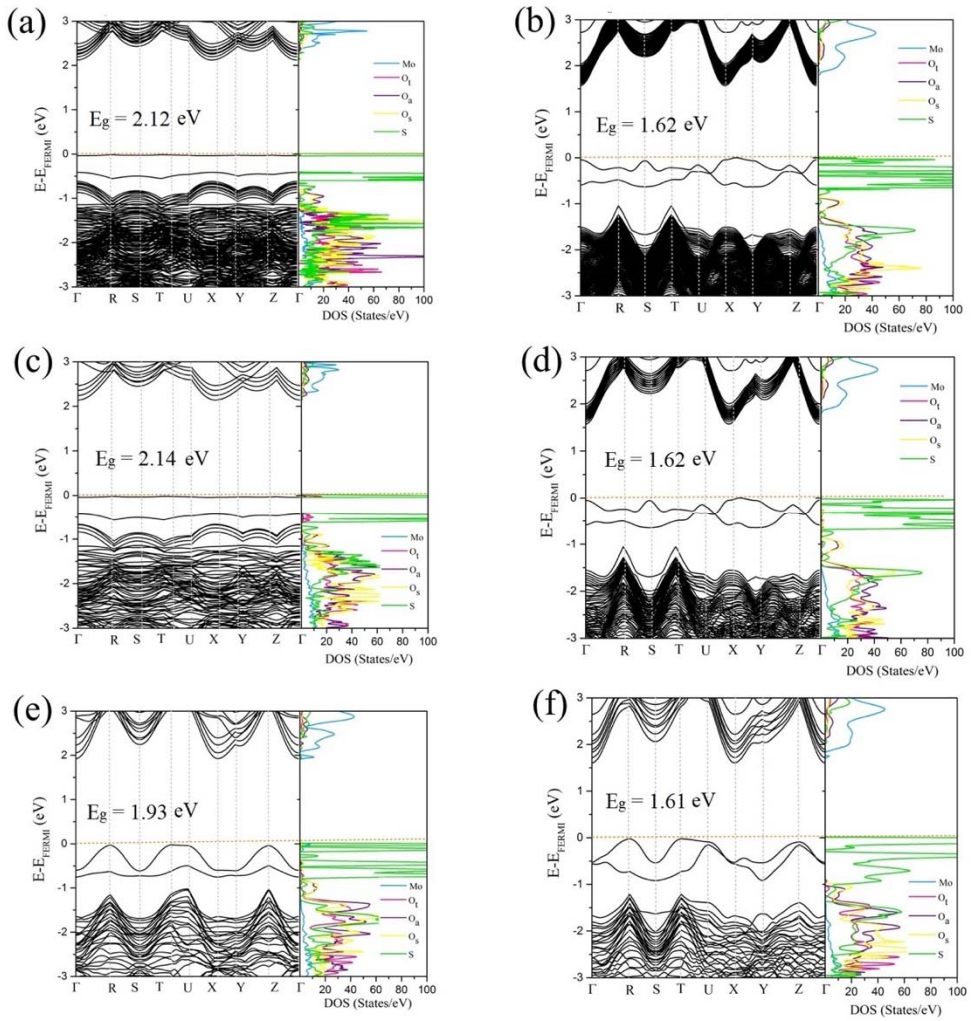

Figure S13. Band structure and PDOS of the fully and partially S-substituted in one layer of α-MoO_3 bulk structures for different concentrations calculated using HSE06. S-substituted (a) (2 × 2 × 2) and (b) (8 × 1× 1) supercells of α-MoO_3 for x_s = 1.04% (with $MoO_{2.97}(S_t)_{0.03}$ chemical formula), (c) (1 × 2 × 2) and (d) (4 × 1× 1) supercells of α-MoO_3 with the S doped for x_s = 2.08% (with $MoO_{2.94}(S_t)_{0.06}$ chemical formula), (e) (2 × 1 × 1) and (f) (1 × 2 × 1) supercells of α-MoO_3 with S doped for x_s = 4.16% (with $MoO_{2.87}$ $(S_t)_{0.13}$ chemical formula). All structures are presented in Fig S2 and S4. The Fermi level is set to zero.

To study the effects of S substitution in different oxygen sites (O_t, O_a and O_s), the band structure and PDOS of S-substituted α-MoO_3 bulk structures for xs = 8.33% at different configurations were calculated as shown in Fig. S14. It can be seen that for S_t substitution, the states are strongly localized and apparently, they are more delocalized for S_s substitution (the S_a is an intermediate structure).

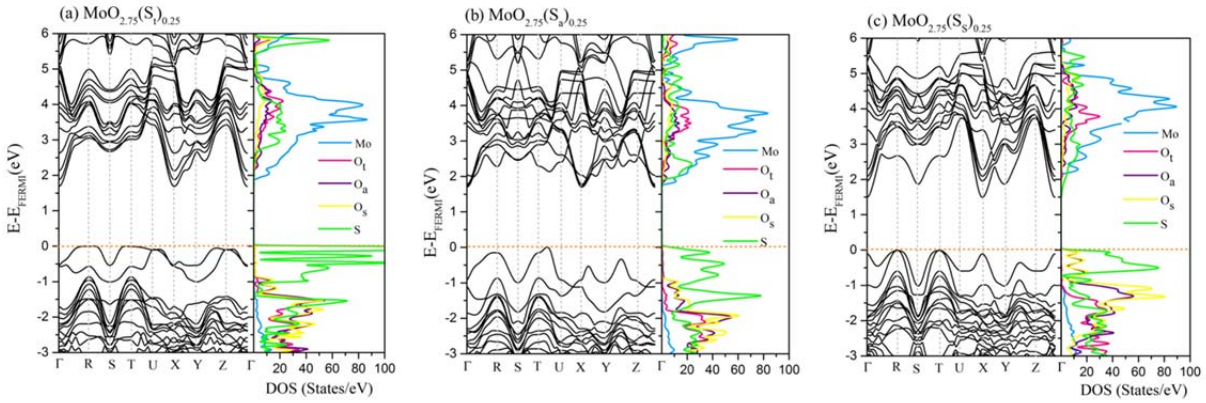

Figure S14. Band structure and PDOS of S-substituted α-MoO_3 bulk structures (x_s = 8.33%) for different configurations: $MoO_{2.75}(S_t)_{0.25}$ (a), $MoO_{2.75}(S_a)_{0.25}$ (b), and $MoO_{2.75}(S_s)_{0.25}$ (c). calculated using HSE06. The Fermi level is set to zero. The related structures are presented in Fig. S3.

Furthermore, we calculated the band structure and PDOS for different configurations (a, b and c in Fig. S5) of S-substituted α-MoO_3 for x_s = 16.66%. Fig. S15 illustrates the band structure and PDOS for aforementioned structures. It is revealed that the delocalization is strong for configuration c (from Fig. S5), when S-atoms are face-to-face, whereas the two other cases (configuration a and b) where S-atoms are facing to O atoms exhibit localized states.

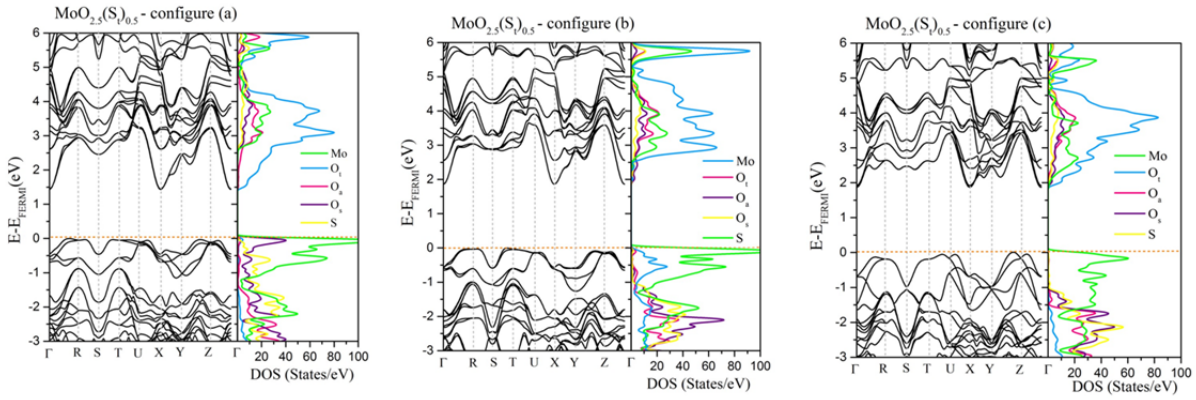

Figure S15. Band structure and PDOS of S-substituted α-MoO_3 bulk structures (x_s = 16.66%) for different configurations as shown in Fig. S5. The Fermi level is set to zero.

4. Electronic properties of Oxygen-doped 2H-MoS_2 in different concentrations

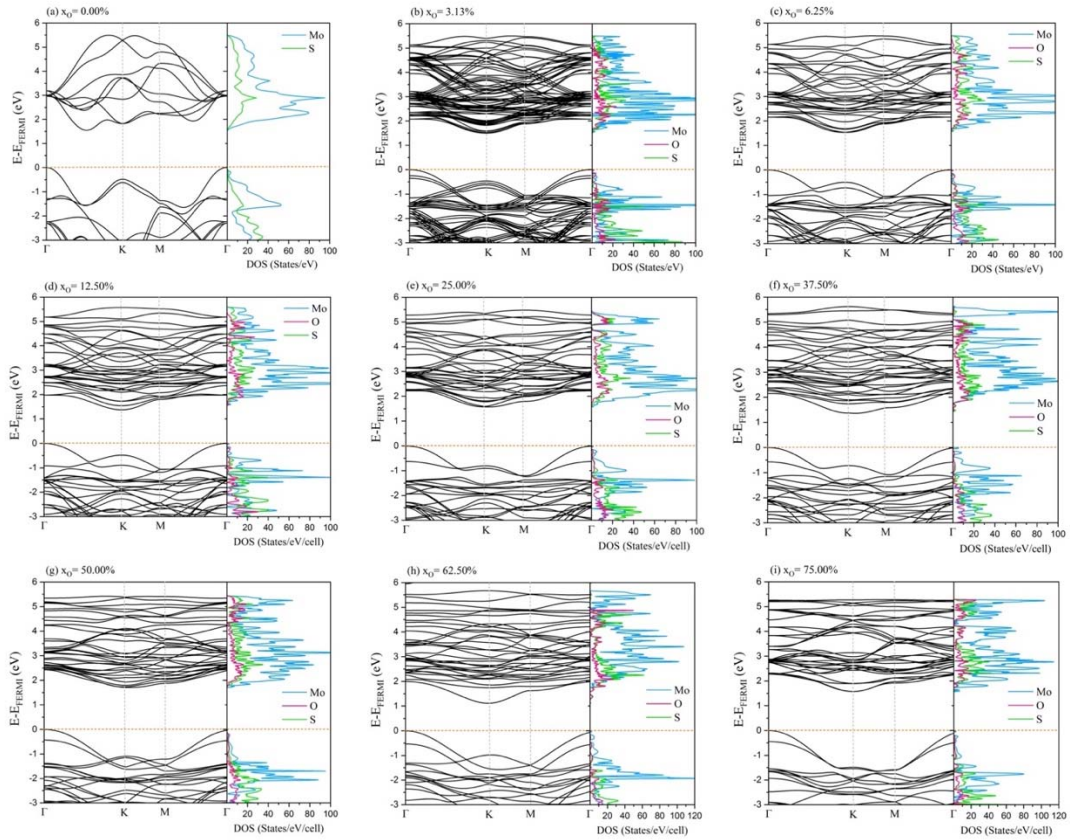

Figure S16. Band structure and PDOS of the most stable O-substituted 2H-MoS_2 bulk structures for different concentrations calculated using HSE06. The Fermi level is set to zero.

Table S4. DFT calculated band gap energy, effective mass of electron and hole, DOS- averaged effective masses, electron and hole mobility of the most stable O-substituted 2H-MoS_2 bulk structures for different concentrations.

System	O concentration (%)	E_g (eV)	m_e^{*a} (m_e)	m_h^{*a} (m_e)	$m_{e\ DOS}^{*b}$ (m_e)	$m_{h\ DOS}^{*b}$ (m_e)	μ_e ($cm^2\ V^{-1}\ s^{-1}$)	μ_h ($cm^2\ V^{-1}\ s^{-1}$)
MoS_2	0.0	1.56	0.82	0.67	0.38	0.23	46	75
$MoS_{1.94}O_{0.06}$	3.13	1.50	0.61	0.67	0.75	0.40	24	46
$MoS_{1.87}O_{0.13}$	6.25	1.54	0.73	0.68	0.37	0.32	47	54
$MoS_{1.75}O_{0.25}$	12.50	1.38	0.52	0.65	0.42	0.81	42	22
$MoS_{1.50}O_{0.50}$	25.00	1.57	0.50	0.65	0.45	0.34	39	52
$MoS_{1.25}O_{0.75}$	37.50	1.38	0.73	0.62	0.56	0.66	31	27
MoSO	50.00	1.71	0.40	0.59	0.40	0.86	44	20
$MoS_{0.75}O_{1.25}$	62.50	1.12	0.73	0.65	2.75	0.83	6	21
$MoS_{0.50}O_{1.50}$	75.00	1.57	0.66	0.70	1.00	0.43	18	40

[a] Harmonic average of [100], [010], [001], [110], [101], [011] and [111] directions. [b] DOS- averaged effective masses and mobility obtained from the Boltzmann transport theory as implemented in CRYSTAL17 code and calculated at a carrier density of 10^{17} cm^{-3}.

We also compared the electronic band gap results for fully substituting S atoms with O atoms in a layer of MoS_2 system (O atoms doped into a 2×2×1 supercell) and partially O-substituted ones (O atoms doped into a unit cell). Figure S17 illustrates the band structure and PDOS for these systems. Our results show that the partially O-substituted 2H-MoS_2 systems in a layer lead to a larger electronic band gap than fully O-substituted ones.

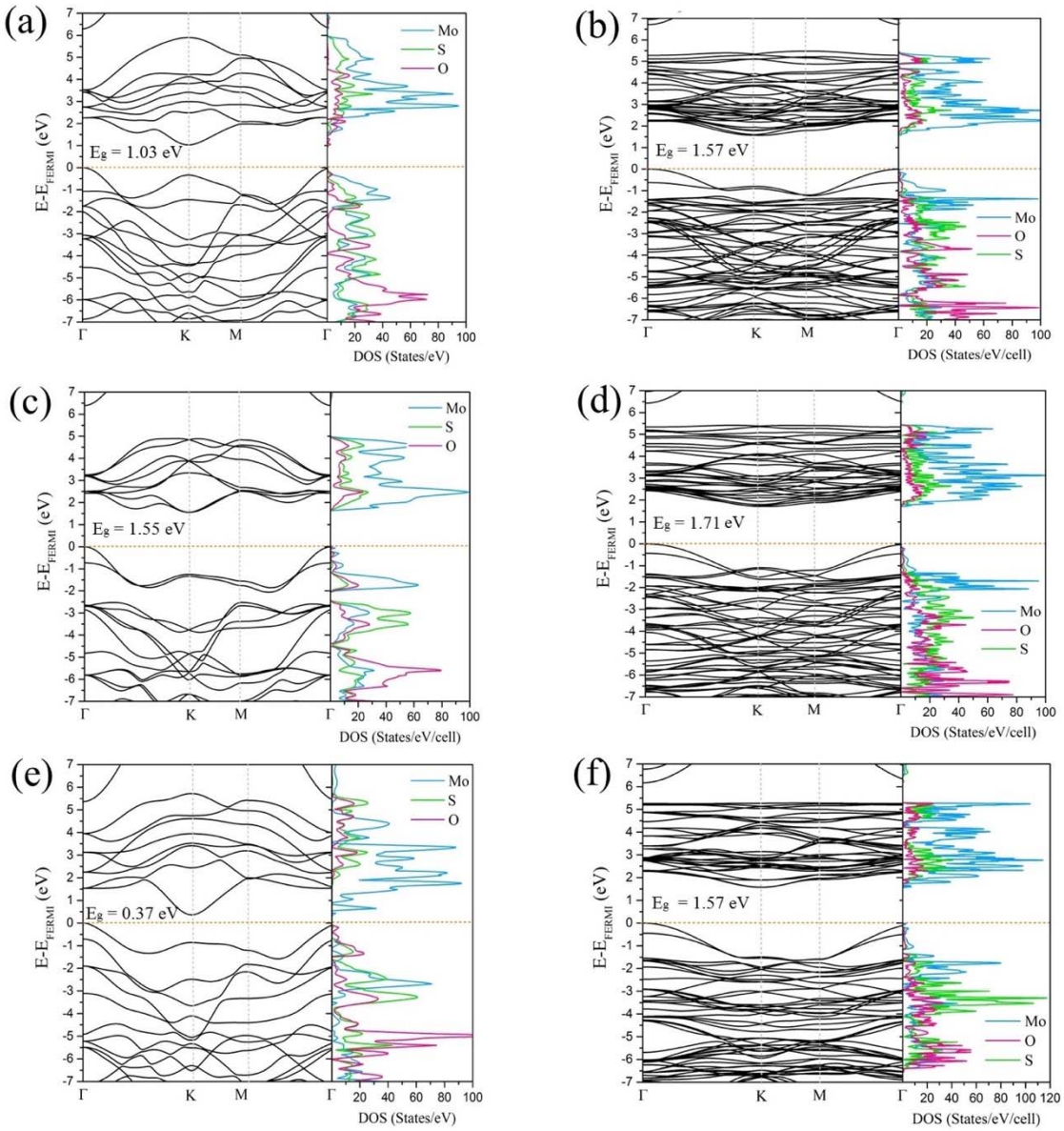

Figure S17. Band structure and PDOS of the fully and partially O-substituted in a layer of 2H-MoS_2 bulk structures for different concentrations calculated using HSE06. (a) MoS_2 unit-cell with x_O = 25.00% ($MoS_{1.50}O_{0.50}$), (b) (2 × 2 × 1) supercell of bulk MoS_2 with x_O = 25.00% ($MoS_{1.50}O_{0.50}$), (c) MoS_2 unit-cell with x_O = 50.00% (MoSO), (d) (2 × 2 × 1) supercell of bulk MoS_2 with x_O = 50.00% (MoSO), (e) MoS_2 unit-cell with x_O = 75.00% ($MoS_{0.50}O_{1.50}$) and (f) (2 × 2 × 1) supercell of bulk MoS_2 with x_O = 75.00% ($MoS_{0.50}O_{1.50}$). All structures are presented in Fig S7 and S8. The Fermi level is set to zero. For x_O = 50.0% (two O-substituted in MoS_2 unit-cell), we only reported the electronic band structure and PDOS for the system with the largest band gap.

5. Absorption coefficient of S-doped α-MoO_3 and O-doped MoS_2 in different concentrations

Due to asymmetric structures of α-MoO_3 and 2H-MoS_2, the optical spectra may show anisotropic behaviors for the light polarizations along different axes (Fig. 1). Hence, the absorption coefficients (α) for all studied systems were also computed along different light polarizations as shown in Fig. S18. It can be seen that the anisotropic behaviors of the two materials differ. Absorption coefficients for S-doped MoO_3 systems along the *a*-axis (Fig. 1), the direction aligned with van der Waals gap, are 5 times higher than in-plane directions whereas it is the reverse for O-doped 2H-MoS_2. The absorption coefficients along both in-plane x- and y-directions (*a*-axis and *b*-axis in Fig. 1) are 5 times higher than those along the z-axis (*c*-axis along vdW gap). From Figs. 4 and S18, it is also obvious that the high absorption coefficients along different polarizations were obtained for these materials in the near-ultraviolet range (NUV, 400 nm down to 300 nm), but it decreased sharply in the visible light region.

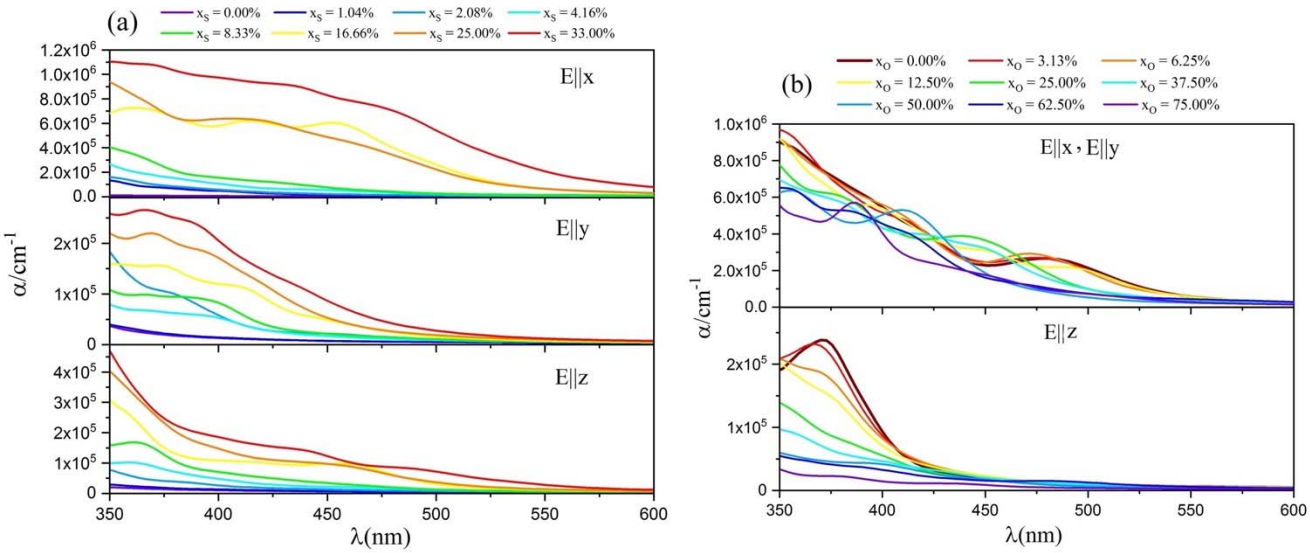

Figure S18. The absorption coefficient (α) of (a) the most stable S-substituted α-MoO_3 bulk structures and (b) the most stable O-substituted 2H-MoS_2 bulk structures at different concentrations for light polarizations along the *x*-, *y*- and *z*-directions correspond to a-, b- and c-axis (as shown in Fig. 1).

6. Charge Transport

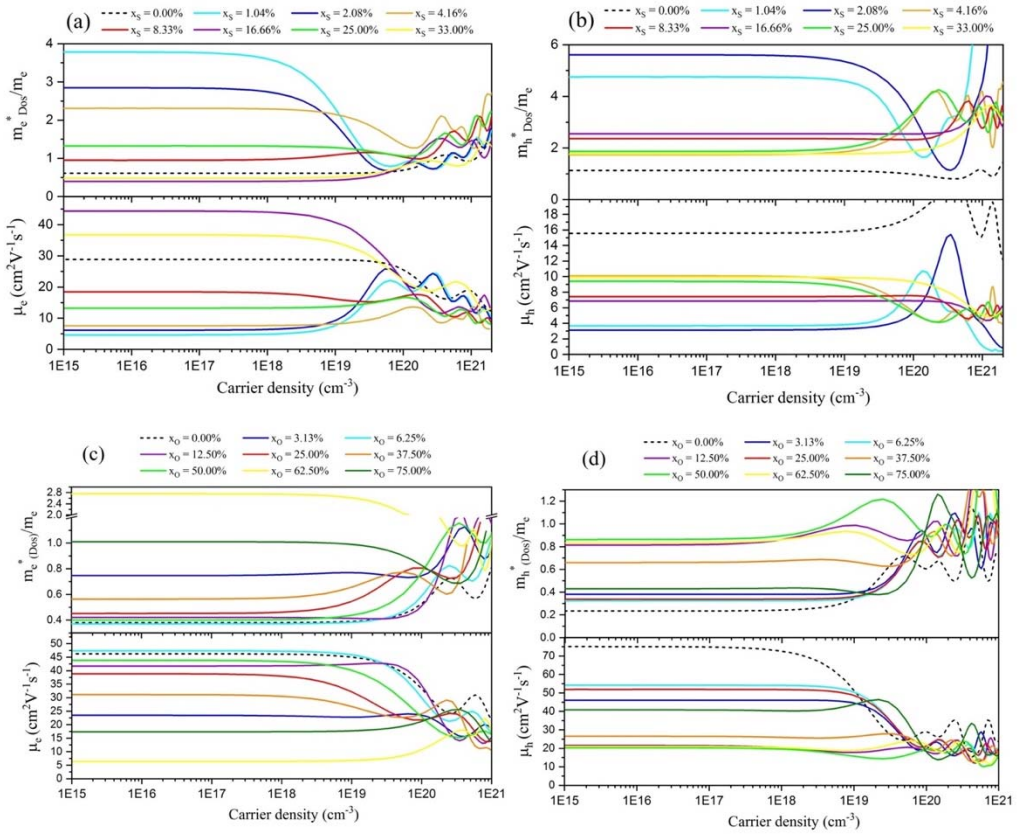

Figure S19. The density-of-states-averaged electron and hole effective mass ($m_{e,h}^{*}{}_{(DOS)}$) and mobility ($\mu_{e,h}$) obtained with the Boltzmann transport theory as a function of the carrier density for (a and b) the most stable S-substituted α-MoO_3 bulk structures and (c and d) the most stable O-substituted 2H-MoS_2 bulk structures for different percentages. A 10 fs scattering time (τ) was assumed at a constant temperature of 300 K.

7. Dielectric constant

Table S5. DFT calculated electronic dielectric constant (ε_∞), relative dielectric constant (ε_r) and exciton binding energy (E_b) of the most stable S substituted α-MoO_3 bulk structures for different concentrations.

System	S concentration (%)	ε_r (ε_∞) E||x	ε_r (ε_∞) E||y	ε_r (ε_∞) E||z	ε_r (ε_∞) Geometric average	E_b (meV)
MoO_3	0.0	6.0 (4.3)	36.5 (6.8)	12.3 (5.9)	13.9 (5.6)	28
$MoO_{2.94}S_{0.06}$	2.08	7.2 (4.5)	56.9 (7.9)	17.8 (6.8)	19.4 (6.2)	69
$MoO_{2.87}S_{0.13}$	4.16	6.5 (4.6)	36.1 (6.9)	13.0 (6.0)	14.5 (5.8)	65
$MoO_{2.75}S_{0.25}$	8.33	6.9 (5.0)	35.7 (6.9)	12.2 (6.2)	14.4 (5.9)	46
$MoO_{2.50}S_{0.50}$	16.66	8.9 (6.2)	34.2 (7.2)	11.8 (6.6)	15.3 (6.7)	20
$MoO_{2.25}S_{0.75}$	25	10.4 (7.2)	33.7 (7.2)	12.0 (6.7)	16.2 (7.1)	47
MoO_2S	33	15.1 (10.1)	32.5 (7.6)	11.6 (7.2)	17.9 (8.2)	16

Table S6. DFT calculated electronic dielectric constant (ε_∞), relative dielectric constant (ε_r), reduced mass (m_r^*) and exciton binding energy (E_b) of the most stable O substituted MoS_2 bulk structures for different concentrations.

System	O concentration (%)	ε_r (ε_∞) E||x	ε_r (ε_∞) E||z	ε_r (ε_∞) Geometric average	E_b (meV)
MoS_2	0.0	14.7 (14.5)	6.4 (6.3)	11.1 (11.0)	16
$MoS_{1.94}O_{0.06}$	3.13	14.7 (14.5)	6.2 (6.2)	11.0 (10.9)	29
$MoS_{1.87}O_{0.13}$	6.25	14.6 (14.4)	6.1 (6.0)	10.9 (10.8)	20
$MoS_{1.75}O_{0.25}$	12.50	14.5 (14.2)	5.81 (5.8)	10.7 (10.5)	34
$MoS_{1.50}O_{0.50}$	25.00	14.0 (13.7)	5.38 (5.4)	10.2 (10.0)	25
$MoS_{1.25}O_{0.75}$	37.50	13.6 (13.3)	4.87 (4.8)	9.7 (9.5)	44
MoSO	50.00	13.0 (12.5)	4.44 (4.4)	9.1 (8.8)	44
$MoS_{0.75}O_{1.25}$	62.50	13.9 (13.1)	4.53 (4.4)	9.6 (9.1)	95
$MoS_{0.50}O_{1.50}$	75.00	13.3 (12.4)	3.92 (3.8)	8.9 (8.4)	71

References

1) S. Grimme, J. Antony, S. Ehrlich, and S. Krieg, *J. Chem. Phys., 2010,* ***132****, 154104.*
2) R. Coehoorn, C. Haas, J. Dijkstra, C. J. F. Flipse, R. A. de Groot, A. Wold, *Phys. Rev. B* 1987, ***35*** (12), 6195–6202.
3) S. N. Steinmann, C. Corminboeuf, *J. Chem. Theory Comput.* 2010, 6 (7), 1990-2001.
4) S. Gautier, S. N. Steinmann, C. Michel, P. Fleurat-Lessard, P. Sautet, *Phys. Chem. Chem. Phys.*, 2015,17, 28921-28930.
5) H. Negishi, S. Negishi, Y. Kuroiwa, N. Sato, S. Aoyagi, *Phys. Rev. B* 2004, ***69*** (6), 064111.
6) Y.-H. Lei, Z.-X. Chen, *J. Phys. Chem. C* 2012, ***116*** (49), 25757–25764.
7) S. Bandaru, G. Saranya, N. J. English, C. Yam, M. Chen, *Sci. Rep.* 2018, ***8*** (1), 10144.
8) G. Henkelman, A. Arnaldsson, H. Jónsson, *Comput. Mater. Sci.* 2006, ***36*** (3), 354–360.
9) B. Radisavljevic, A. Radenovic, J. Brivio, V. Giacometti, A. Kis, *Nat. Nanotechnol.* 2011, ***6*** (3), 147–150.
10) K. F. Mak, C. Lee, J. Hone, J. Shan, T. F. Heinz, *Phys. Rev. Lett.* 2010, ***105*** (13), 136805.
11) T. Le Bahers, K. Takanabe, *J. Photochem. Photobiol. C Photochem. Rev.* 2019, ***40***, 212–233.